AIP Physics of Plasmas

Laser generated proton beam focusing and high temperature isochoric heating of solid matter

R. A. Snavely, B. Zhang, K. Akli, Z. Chen, R. R. Freeman et al.

Citation: Phys. Plasmas **14**, 092703 (2007); doi: 10.1063/1.2774001
View online: http://dx.doi.org/10.1063/1.2774001
View Table of Contents: http://pop.aip.org/resource/1/PHPAEN/v14/i9
Published by the American Institute of Physics.

Laser generated proton beam focusing and high temperature isochoric heating of solid matter

R. A. Snavely,[1] B. Zhang,[2,a)] K. Akli,[2] Z. Chen,[3] R. R. Freeman,[4] P. Gu,[4] S. P. Hatchett,[1] D. Hey,[2] J. Hill,[4] M. H. Key,[1] Y. Izawa,[3] J. King,[2] Y. Kitagawa,[3] R. Kodama,[3] A. B. Langdon,[1] B. F. Lasinski,[1] A. Lei,[3] A. J. MacKinnon,[1] P. Patel,[1] R. Stephens,[5] M. Tampo,[3] K. A. Tanaka,[3] R. Town,[1] Y. Toyama,[3] T. Tsutsumi,[3] S. C. Wilks,[1] T. Yabuuchi,[3] and J. Zheng[3]

[1]*University of California, Lawrence Livermore National Laboratory, P.O. Box 808, Livermore, California 14550, USA*

[2]*University of California, Davis, Department of Applied Science, P.O. Box 808, L714, Livermore, California 94552 USA*

[3]*Institute of Laser Energetics, Osaka University, Suita, Osaka 565, Japan*

[4]*The Ohio State University, Columbus, Ohio 14320 USA*

[5]*General Atomics, San Diego, California 13286 USA*

(Received 2 January 2007; accepted 18 July 2007; published online 21 September 2007)

The results of laser-driven proton beam focusing and heating with a high energy (170 J) short pulse are reported. Thin hemispherical aluminum shells are illuminated with the Gekko petawatt laser using 1 μm light at intensities of $\sim 3\times 10^{18}$ W/cm^2 and measured heating of thin Al slabs. The heating pattern is inferred by imaging visible and extreme-ultraviolet light Planckian emission from the rear surface. When Al slabs 100 μm thick were placed at distances spanning the proton focus beam waist, the highest temperatures were produced at 0.94× the hemisphere radius beyond the equatorial plane. Isochoric heating temperatures reached 81 eV in 15 μm thick foils. The heating with a three-dimensional Monte Carlo model of proton transport with self-consistent heating and proton stopping in hot plasma was modeled. © *2007 American Institute of Physics*.

[DOI: 10.1063/1.2774001]

I. INTRODUCTION

Fast ignition (FI) of thermonuclear fusion is an attractive scheme to increase the energy gain, reduce the laser driver energy, and relax fuel compression uniformity in inertial confinement fusion.[1] Recent work has demonstrated >20% efficient coupling of picosecond pulse laser energy to a compressed core through fast electrons.[2] The transport of energy by the electrons is subject to complex effects from self-consistent *E* and *B* fields, which could reduce the efficiency in full-scale fast ignition.

Shortly after the first observations of collimated laser-generated proton plasma jets[3] it was suggested that protons could offer an alternative path to FI with simpler energy transport physics.[4,5] While there are several mechanisms of laser acceleration of protons,[6–10] that leading to focusing is proton plasma expansion driven by hot electron pressure[11] perpendicular to a concave surface. The first demonstration of generation of a focused proton plasma jet from the inner surface of a thin tightly curved hemi-shell and of isochoric heating (in time short relative to hydrodynamic expansion time)[12] was made using a 10 J, 0.1 ps laser system.[13] The results suggest both that proton isochoric heating offers new possibilities in high energy density physics through creating unique states of matter and that fast ignition with protons merits further study.

Modeling predicts that the FI requirement at a typical FI deuterium tritium fuel density of 300 g/cm^3 is to deliver 20 kJ of protons into 40 μm diameter spot with a suitable Boltzmann-like energy spectrum (kT=3 to 5 MeV).[14–16] For a practical feasibility the laser to hot spot energy coupling efficiency should be >10%. The fact that conversion of short pulse laser energy to proton beam energy has reached efficiencies >10%[3,11] is encouraging.

II. EXPERIMENTAL CONFIGURATION

Here we describe proton focusing experiments with 20× higher energy than was used in the initial experiments. We used the Gekko petawatt (PW) Laser System at ILE–Osaka University.[17] It delivered pulses of 700 fs duration with an average of 170 J on target. The targets had two parts illustrated in Fig. 1: a hemispherical Al shell 360 μm diameter with 13–16 μm thickness, which was illuminated by the laser pulse on its exterior pole and generated the proton beam from its inner shell surface, and an Al slab of thickness 15 to 100 μm for proton beam stopping and heating mounted close to the hemisphere on a stalk. The laser was focused with an $f/10$ mirror with a spot size of 40×60 μm estimated from x-ray pinhole camera images, giving an intensity of $\sim 3\times 10^{18}$ W/cm^2.

Three main diagnostics were used, as shown in Fig. 1: two imaged the Planckian emission from the rear surface of the heated foil in the visible and extreme-ultraviolet light (XUV). A time-integrated XUV imaging microscope[18] had a band pass of 8 eV centered at 68 eV. It used Mo_2C:Si multilayer mirrors. The focal length of the spherical primary

a)Electronic mail: bbzhang@ucdavis.edu

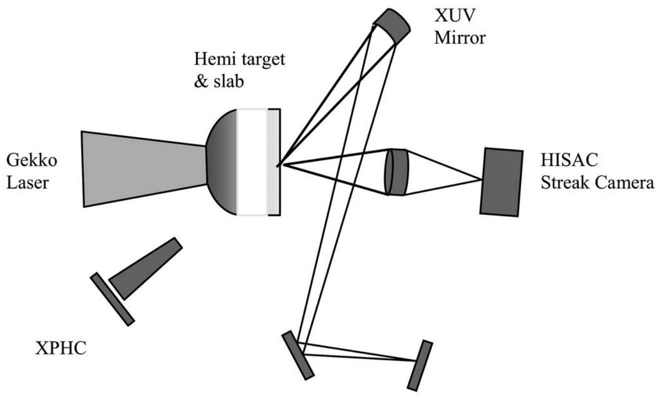

FIG. 1. Schematic of experiment. Positions of XUV, HISAC, and x-ray pinhole cameras.

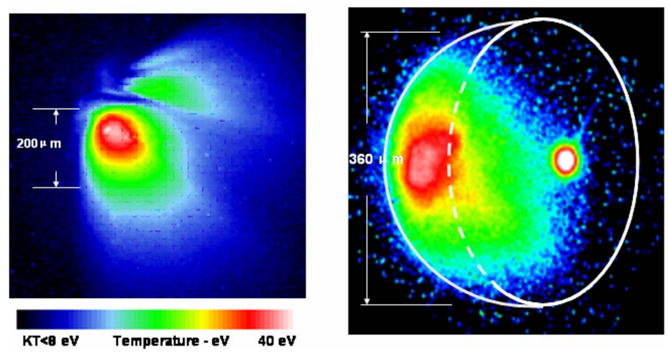

FIG. 2. (Color online) (Left) XUV image of proton heating of a 60 μm Al foil at D/r=1.5, converted to temperature. (Right) X-ray pinhole camera image of a laser irradiated Al hemisphere with a 100 μm thick Al foil at D/r=1.8.

mirror was 308 mm and a 45° flat turning mirror was included for stray light suppression.

The XUV magnification was 10.2 or 13.1 and the measured resolution was <10 μm. The viewing angle was 41° from the normal to the rear target surface. A Princeton Instruments cooled CCD camera (SITE CCD back-thinned and back-illuminated 1k×1k) recorded the XUV image. The XUV imaging channel was absolutely calibrated.[18] The 68 eV mirrors were calibrated with synchrotron radiation source at Brookhaven National Laboratory. Mirror reflectivity was obtained with a pair of diodes measuring the incoming XUV and the reflection off the mirrors. An Fe55 radioactive source was used to calibrate CCD cameras. The number of counts on a pixel produced by absorption of a photon at the CCD camera was carefully measured.

A high-speed optical imaging streak camera (HISAC) imaged the rear surface at 15° from the normal in the spectral range 400–700 nm. A notch filter between 500 and 550 nm was used to block imaging of 2ω transition radiation. It produces gated images in a 10×10 pixel array with 45 μm spatial resolution and 50 ps temporal resolution using a multichannel fiber optic technique.[19] The images are constructed by two-dimensional (2D) interpolation between pixels from the optical streak signal. Thus, the HISAC images were obtained from the first 50 ps of Planckian emission.

A time-integrated x-ray pinhole camera with a 20 μm diameter aperture and a 20 μm thick Be filter imaged the x rays from the front of the laser target interaction region at an angle of 35° to the laser.

III. EXPERIMENTAL RESULTS

To study the focusing, we varied two parameters for this experiment. Either we moved a 100 μm thick Al slab along the axis within the focal region of the proton plasma jet or we fixed the distance and varied the Al thickness.

We used a simple model based on measured proton source diameters and proton plasma jet divergence measurements from planar foil targets to infer the location of the best focus from a spherically bent foil. The model assumed the angle of the flow relative to the normal to the surface as a function of the radius is the same in both cases.[13] For the focusing study, the placement of the Al slab [the side toward the hemi-shell] relative to the pole of the hemisphere was in the range 1.25 to 2.5 times the hemisphere radius. We characterize the targets with this ratio D/r, where D is the distance from the apex of the hemi-shell to the rear surface of the secondary Al foil and r is the radius of the hemisphere.

Typical analyzed data from the XUV microscope are shown in Fig. 2 (left). The 41° oblique view of the heated region shows a bright XUV emission spot and a weaker secondary spot, converted to a map of temperature with a peak of 42 eV and a sensitivity floor of 8 eV. There is also an expansion plume to the right along the target normal direction due to the oblique view and time-integrated XUV image acquisition. The image is transformed into temperature via a numerical model and absolute calibration discussed later. Figure 2 (right) shows an x-ray pinhole camera image. The 40×60 μm laser focal spot is seen in the upper left. The size is consistent with previous spot measurements. Electron refluxing in the hemisphere produces thermal x-rays over a broader region than the laser focal spot outlining the hemisphere. An intense saturated spot (radius <20 μm) is seen in the proton focal region on the front surface of the 100 μm thick Al slab. This image is recorded in transmission of x rays through the Al hemispherical shell laser target and implies a temperature of ~200 eV, as discussed later. Similar data also showed a double peak of proton heating, which correlated with a double peak of x-ray emission from the irradiated hemisphere. This suggests that observation of multiple proton heating peaks in this experiment is due to inhomogeneity of irradiation, which distorts the topology of the Debye sheath and perturbs the local direction of proton acceleration.[20]

Temperature measurements

The 68 eV emission is optically thick at 0.1 μm depth in solid Al, so that the recorded image is from heating close to the rear surface. The rear surface temperature was deduced from the absolute brightness of the XUV Planckian emission.[18] We compared the time-integrated emission with a one-dimensional (1D) model calculated with the radiation-hydrodynamics code LASNEX.[21] The XUV opacities in these calculations were derived from the super-transition array formalism[22,23] and also from an in-line, average atom

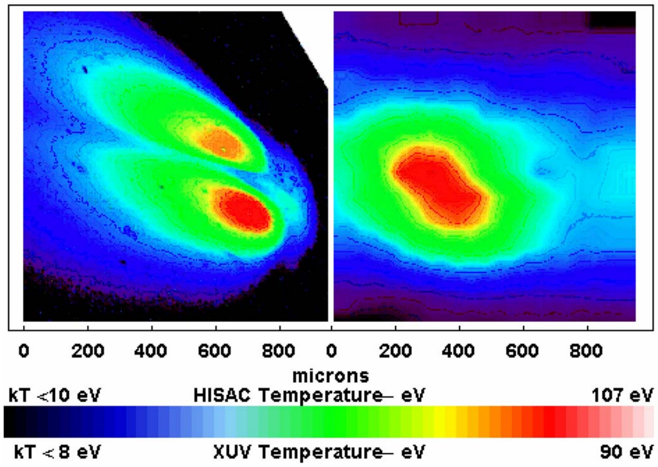

FIG. 3. (Color online) XUV (left) and HISAC (right) comparison of temperature maps of the same shot at $D/r=1.74$ corrected geometrically to have same spatial scale and angle of view normal to the surface.

method.[24] We found little sensitivity to which opacity model was used. In the 1D model an infinitely wide aluminum slab, of the same thickness as was used in the experiment, was given a range of initial temperatures T_0 and allowed to expand and cool both adiabatically and radiatively. The calculated, time-integrated, bandpass-integrated intensities, in the same direction with respect to the slab normal as in the experiment, were then compared to the observations. This procedure yields a transformation from XUV intensity to T_0. The sensitivity of the integrated brightness to the finite target thickness effects is very minor compared to the sensitivity to the initial temperature.

Similar calibration was employed for HISAC as summarized in Ref. 19. Figure 3 compares deduced temperature maps for heating a 100 μm thick Al slab with a $D/r=1.74$. Given that HISAC has a limited resolution of ~45 μm, there is a fair correlation between the two temperature maps. The HISAC image blurs the XUV double spot structure. However the geometrical projection and orientation correction for viewing normal to the target surface cannot remove the apparent plume from the XUV data. However, the orientation, scale, structure, and peak temperature of the two images are otherwise consistent.

The XUV data for 13 shots of the focal plane scan with 100 μm thick Al slabs are shown in Fig. 4. The stopping thickness for 3.5 MeV protons normally incident from the front surface is 100 μm Al, so the recorded image is dominated by protons of energy close to 3.5 MeV.[3,11] The highest temperature produced at the rear surface of the 100 μm foil was 81 eV. The temperature data are normalized for shot to shot variance of the laser energy by dividing temperature by the laser energy and multiplying by the mean laser energy. The energy on target was approximately 60% of the energy from the final amplifier due to losses in the grating compressor and focusing optic. The on-target mean energy was 285 J with an RMS variation of 47.3 J (30% of this energy was within the laser focal spot). Two shots at the D/r ratio of 1.25 did not produce an XUV image. The CCD noise floor puts an upper bound temperature on these shots of 8 eV. A Gaussian fit shows the best focusing of the 3.5 MeV protons at a D/r ratio of 1.94 ± 0.4. The Poisson error in the temperature is deduced from the number detected quanta in each CCD pixel, Poisson errors for all the shots are less than 1 eV, and the error bars are too small to be shown in Fig. 4. The scattered data shown in Fig. 4 are due to systematic errors that we can not control; e.g., the error from the target alignment and variability of the laser focal spot. The temperature profile diameters [full width at half-maximum (FWHM)] were measured in both horizontal and vertical directions and then averaged. This minimizes inclusion of plasma plume expansion in the estimation. For data where there are multiple spots, the FWHM of the heating was deduced from the largest radius points at half the peak intensity. Figure 4 (top) shows the radii as a function of D/r. We find a minimum proton plasma jet waist with an average diameter of 206 μm at $D/r=1.8\pm0.4$. This is significantly wider than was observed with a more uniform and smaller focal spot on the hemi-shell.[13] In

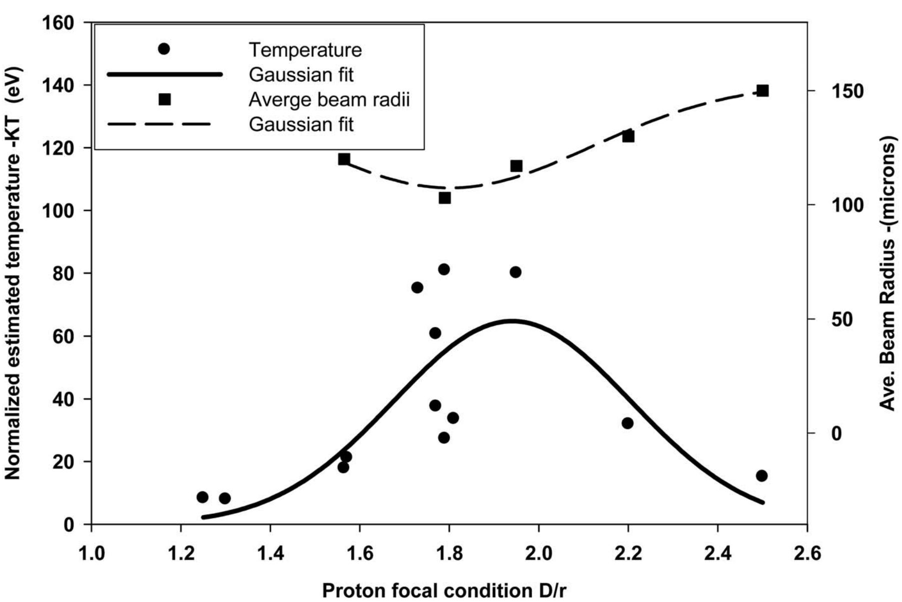

FIG. 4. Filled circles: peak XUV temperatures normalized to the average laser energy with 100 μm thick Al targets. Filled squares: averaged radii of the heated spot at half-peak temperature.

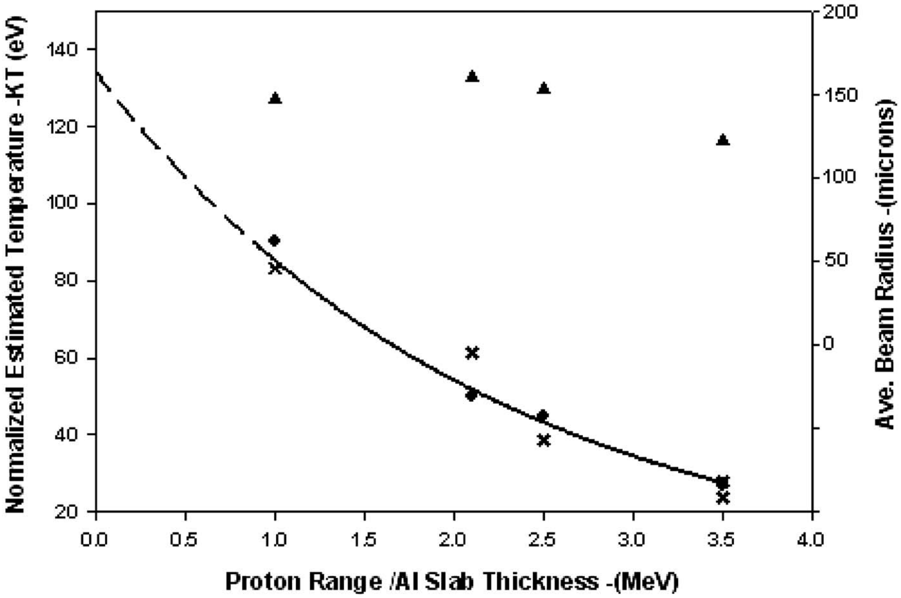

FIG. 5. Crosses: Peak temperatures normalized to the average laser energy at D/r of 1.5. Line: a simple model fit for a Boltzmann temperature of 2.2 MeV. Dots: a 3D Monte Carlo simulation discussed in the text. Triangles: averaged beam radii.

our work the proton plasma jet was structured and wider and we attribute this to structure in the focal spot pattern, as noted in Sec.III.

A second set of data measured the variation of peak temperature with a change in the Al slab thickness with a fixed D/r ratio of 1.5. The D/r ratio was chosen prior to the experimental determination of optimal D/r of 1.94. The Al slab thickness determines the energy band of protons inducing the majority of the heating.[3,11] We used Al slab thickness (proton energy) of 100 μm (3.5 MeV), 60 μm (2.5 MeV), 47 μm (2.1 MeV), and 15 μm (1 MeV). The results are shown in Fig. 5.

There is a trend to increased heating at reduced thickness. The highest recorded peak temperature is 83 eV for 15 μm (1 MeV) thickness after being normalized to the average laser energy of 359 J.

A simple model fit to the proton data shown as a line in Fig. 5 gives a Boltzmann temperature of 2.2 MeV and thus implies a front surface temperature $\sim$132 eV. The model assumes that protons deposit their energy at their Bragg peak that is narrow relative to the slope temperature and that their range increases quadratically with energy.

The very bright spot evident in the x-ray pinhole camera image of Fig. 2 gives another estimation of the front surface temperature. The emission from the front surface of the Al slab is filtered by the Al hemi-shell and the Be filter. The x-ray transmission is appreciable only for x rays of energy greater than $\sim$900 eV, consistent with a front surface temperature of 200 to 300 eV on this shot. The higher temperature may be due to heating by other fast ions and co-moving electrons. Other fast ions with higher charge and mass have a very short range and can cause strong surface heating. Co-moving electrons which have much lower kinetic energy and shorter range will contribute their energy to the front surface for thick Al slabs, but will have some effects for very thin Al foils (15 μm Al slab in our experiment).

Regarding our method of determining temperature via 1D simulation of the XUV emission, some caution must be observed. There are two potentially significant effects, which we have ignored: lateral expansion and initial temperature gradients from the exponential proton spectrum in the solid Al. The protons only heat a finite spot. In the XUV "pictures," this spot is wider than the slab thickness, so the initial expansion is roughly 1D. Nevertheless, the pictures show plume structures apparently expanding away from the initial hot spots. Hence, the XUV camera is looking through the side of the plume and the expansion must be 2D or 3D, with more adiabatic cooling and a steeper density gradient in the rarefaction.

We performed several calculations to test the model sensitivity to the above effects. The overwhelming sensitivity of the observed integrated intensity is to T_0: it scales roughly as T_0^3 in the range of 20–200 eV. The lateral expansion effect seen in 2D calculations is almost negligible for the observed spot sizes and T_0 in the range of 20–60 eV; at higher T_0 the effect increases, reducing the intensity seen for 100 eV by about 50%, still resulting in only a modest temperature error.

IV. MONTE CARLO MODEL OF PROTON HEATING

To estimate the energy content of the proton plasma jet and its energy spectrum we constructed a 3D Monte Carlo proton transport and dose code with self-consistent heating, explicit equation of state (EOS), and hot stopping powers for the protons.[25] We used a simple hot stopping model[25] with a SESAME EOS together with a collisional code kernel.[26] Following the prescription in Mehlhorn,[25] a mean ionization potential $\langle I \rangle$ was calculated for an effective Z, and the cold stopping powers were adjusted for this effective Z and $\langle I \rangle$ to give the bound stopping in warm material. We assumed a Boltzmann spectrum and a Gaussian transverse intensity. The area$\times$temperature integral $\int T da$ in the model was the same as that determined from the XUV images at best focus after these images were transformed to temperature plots. The protons were sent into the target in order of decreasing energy to mimic the time-of-flight characteristic dependence laser-driven protons. The protons entered the aluminum at normal incidence. The model temperature and total energy were varied to fit the experimental data in Fig. 5 leading to a kT of 2 MeV, in agreement with the simple model, and total proton energy of 5.4 J. The average laser energy on target was 173 J, so the conversion efficiency from laser to proton energy was 3.1%.

V. SUMMARY

We have measured the 2D spatial pattern of isochoric heating of Al foil targets by focused laser-driven proton plasma jets. There is a demonstrated temperature peak and beam waist at 0.94 times the hemisphere radius away from the equatorial plane. Peak temperatures reached 83 eV. We deduced the proton energy spectrum to have a Boltzmann temperature of 2 MeV and energy content 3.1% of the laser energy.

ACKNOWLEDGMENTS

This project is supported by the US Office of Fusion Energy Sciences under Contract No. AT5015033. This work was performed under the auspices of the U.S. Department of Energy by the University of California, Lawrence Livermore National Laboratory under Contract No. W-7405-Eng-48.

[1]M. Tabak, J. Hammer, M. E. Glinsky, W. L. Kruer, S. C. Wilks, J. Woodworth, E. M. Campbell, M. D. Perry, and R. J. Mason, Phys. Plasmas **1**, 1626 (1994).
[2]R. Kodama, P. A. Norreys, K. Mima *et al.*, Nature **412**, 798 (2001).
[3]R. A. Snavely, M. H. Key, S. P. Hatchett *et al.*, Phys. Rev. Lett. **85**, 2945 (2000).
[4]M. Roth, T. E. Cowan, M. H. Key *et al.*, Phys. Rev. Lett. **86**, 436 (2001).
[5]M. H. Key, R. R. Freeman, S. P. Hatchett, A. J. Mackinnon, P. K. Patel, R. A. Snavely, and R. B. Stephens, Fusion Sci. Technol. **49**, 440 (2006).
[6]G. Pretzler, A. Saemann, A. Pukhov *et al.*, Phys. Rev. E **58**, 1165 (1998).
[7]M. Zepf, M. Castro-Colin, D. Chambers *et al.*, Phys. Plasmas **3**, 3242 (1996).
[8]K. Codling and L. J. Frazinski, Contemp. Phys. **35**, 243 (1994).
[9]T. Ditmire, J. Zweiback, V. P. Yanovsky, T. E. Cowan, G. Hays, and K. B. Wharton, Nature **398**, 489 (1999).
[10]K. Krushelnick, E. L. Clark, M. Zepf *et al.*, Phys. Plasmas **7**, 2055 (2000).
[11]S. P. Hatchett, C. G. Brown, T. E. Cowan *et al.*, Phys. Plasmas **7**, 2076 (2000).
[12]J. C. Olson, H. A. Davis, and W. J. Waganaar, IEEE Trans. Plasma Sci. **24**, 65 (1996).
[13]P. K. Patel, A. J. Mackinnon, M. H. Key, T. E. Cowan, M. E. Foord, M. Allen, D. F. Price, H. Ruhl, P. T. Springer, and R. Stephens, Phys. Rev. Lett. **91**, 125004 (2003).
[14]R. Ramis and J. Ramirez, Nucl. Fusion **44**, 720 (2004).
[15]M. Temporal, J. J. Honrubia, and S. Atzeni, Phys. Plasmas **9**, 3098 (2002).
[16]S. Atzeni, M. Temporal, and J. J. Honrubia, Nucl. Fusion **42**, L1 (2002).
[17]Y. Kitagawa, Y. Sentoku, S. Akamatsu *et al.*, Phys. Plasmas **9**, 2202 (2002).
[18]P. Gu, B. Zhang, M. H. Key *et al.*, Rev. Sci. Instrum. **77**, 113101 (2006).
[19]R. Kodama, K. Okada, and Y. Kato, Rev. Sci. Instrum. **70**, 625 (1999).
[20]J. Fuchs, T. E. Cowan, P. Audebert *et al.*, Phys. Rev. Lett. **91**, 255002 (2003).
[21]G. B. Zimmerman and W. L. Kruer, Comments Plasma Phys. Controlled Fusion **2**, 51 (1975).
[22]A. Bar-Shalom, J. Oreg, W. H. Goldstein, D. Shvarts, and A. Zigler, Phys. Rev. A **40**, 3183 (1989).
[23]T. Blenski, A. Grimaldi, and F. Perrot, Phys. Rev. E **55**, R4889 (1997).
[24]W. A. Lokke and W. H. Grasberger, in Lawrence Livermore National Laboratory Report No. UCRL-52276, 1977. Copies may be ordered from National Technical Information Service, Springfield, VA 22161
[25]T. A. Mehlhorn, J. Appl. Phys. **52**, 6522 (1981).
[26]J. F. Ziegler, J. P. Biersack, and U. Littmark, *The Stopping and Range of Ions in Solids* (Pergamon, New York, 1985).